OPEN ACCESS

PRZEGLĄD ELEKTROTECHNICZNY

Marcin FRONC[1], Bartłomiej STEFAŃCZAK[2]
ORCID: [1]0009-0004-7970-1148; [2]0000-0001-7071-9131
DOI: 10.15199/48.2025.08.23

Experimental identification the equivalent parameters of a sodium-ion cell

Eksperymentalna identyfikacja parametrów zastępczych ogniwa sodowo-jonowego

[1] mgr inż. Marcin Fronc, Department of Electrical Drives and Machines, Lublin University of Technology, Nadbystrzycka Street 38A, 20-618 Lublin, e-mail: m.fronc@pollub.pl
[2] mgr inż. Bartłomiej Stefańczak, Department of Electrical Drives and Machines, Lublin University of Technology, Nadbystrzycka Street 38A, 20-618 Lublin, e-mail: b.stefanczak@pollub.pl
adres do korespondencji: m.fronc@pollub.pl

Abstract: The article presents the development of a sodium-ion cell model that accurately reproduces the voltage behavior under various operating conditions. To determine the model parameters, experiments were conducted, including measurements of resistance, open-circuit voltage, and cell capacity at different SOC levels, temperatures, and load currents. The developed model allows for precise voltage forecasting of the cell under both high and low load currents. Experimental results were compared with simulations, enabling the evaluation of the model's accuracy, which can be implemented in BMS systems for electromobility and energy storage.

Keywords: cell model, sodium ion cell, internal resistance, dynamic resistance

Streszczenie: Artykuł przedstawia opracowanie modelu ogniwa sodowo-jonowego, który dokładnie odwzorowuje zachowanie napięcia w różnych warunkach roboczych. Do określenia parametrów modelu przeprowadzono eksperymenty, obejmujące pomiar rezystancji, napięcia obwodu otwartego oraz pojemności ogniwa przy różnych poziomach SOC, temperaturach i prądach obciążenia. Opracowany model umożliwia precyzyjne prognozowanie napięcia ogniwa zarówno przy dużych, jak i małych prądach obciążenia. Wyniki eksperymentalne porównano z symulacjami, co pozwoliło ocenić dokładność modelu, który może być zaimplementowany w systemach BMS dla elektromobilności i magazynowania energii.

Słowa kluczowe: model ogniwa, ogniwo sodowo-jonowe, rezystancja wewnętrzna, rezystancja dynamiczna

Introduction

The decarbonization of the energy sector, as well as the implementation of smart-grid and vehicle-to-grid technologies, also represent key components of long-term environmental and energy-related objectives.[1] These policies highlight governments' commitment to creating a sustainable and clean future for transportation. [2]

Such a rapid growth in the electric and hybrid vehicle shown in the graph in Figure 1. market is accompanied by a tremendous demand for batteries, which constitute a significant portion of the total vehicle cost. For this reason, manufacturers are seeking alternative solutions to remain competitive in the market. Sodium-ion (Na-ion) cells [3] are being developed as an alternative to lithium-ion (Li-ion) cells in electric vehicles. In 2023, the first electric car with a Na-ion cell-based battery—the Sehol E10X featuring a 25 kWh battery—was introduced in China. Current literature reports the energy density of sodium-ion cells at approximately 120 Wh/kg [4], although leading Na-ion cell manufacturers, such as CATL, claim values reaching up to 180 Wh/kg [5]. Further development of sodium-ion cell technology is focused on increasing their energy density to 200 Wh/kg [3].

Another factor enhancing the appeal of sodium-ion cells is their resistance to temperature fluctuations. Lithium-ion cells currently in use require maintaining an optimal operating temperature. In addition, the cells that make up the energy storage are subjected to varying load conditions [6]. At low temperatures, their energy delivery capacity significantly decreases [7]. This issue is often addressed by using part of the stored battery energy to heat it [8]. However, this is a suboptimal solution that reduces the overall efficiency of the system. Studies on sodium-ion cells show that low op-

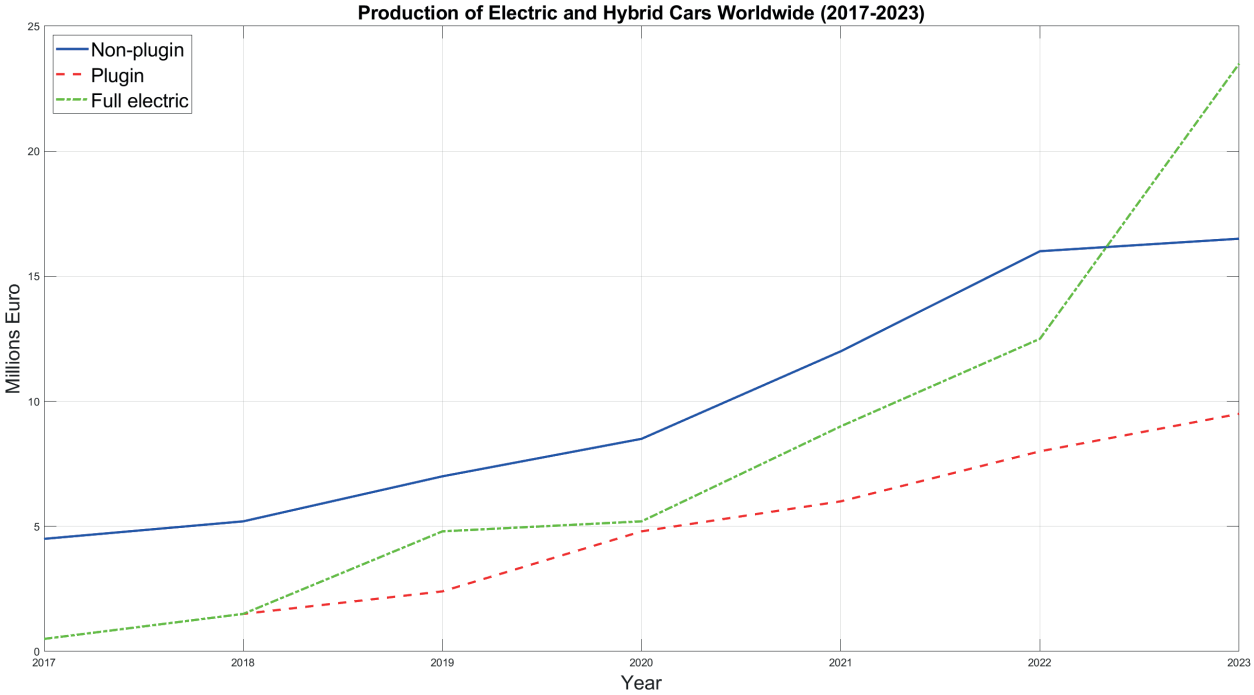

Fig. 1. Production of Electric and Hybrid Cars Worldwide.

erating temperatures have a much smaller impact on their energy delivery capacity [9], [10] compared to lithium-ion cells. At high temperatures, however, sodium-ion cells behave uncontrollably, similar to lithium-ion cells [11], [12], [13].

The safety of electrochemical cells can be determined based on thermal runaway propagation rates shown in the graph in Figure 2. The thermal runaway propagation rates of lithium-ion and sodium-ion cells are well-documented in the literature [11], [14]. The average mass loss rate indicates a significantly slower thermal runaway process [15] in sodium-ion cells compared to nickel-manganese-cobalt cells. Additionally, the temperature rise is twice as slow, although it remains higher than in lithium-iron-phosphate cells [16]. Currently, efforts are underway to develop solutions that enhance the safety of sodium-ion cells [17].

The thermal runaway process in cells is associated with the occurrence of internal short circuits caused by high temperatures, the uncontrolled release of energy stored within, and the subsequent ignition of the electrolyte and electrode materials [18].

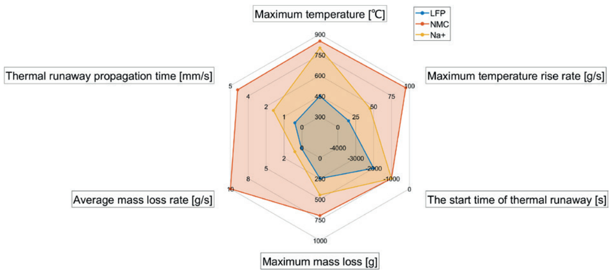

Fig. 2. Comparision thermal runaway between lithium-ion and sodium-ion battery.

Identification of Battery Model Parameters

The Thevenin model of a lithium-ion cell is a simplified electrical model that describes the cell's behavior based on parameters representing its dynamic and static properties [19]. Literature on the modeling of electrochemical cells presents various cell models tailored to different levels of application complexity [20]. For applications utilizing static cell parameters, the use of a series model is justified [21]. However, dynamic load variations require the adoption of more advanced models that account for cell polarization changes [22], [23].

In this study, a first-order equivalent circuit model (Fig. 3b) has been adopted, as it provides satisfactory modeling accuracy.

Figure 3 illustrates the adopted equivalent cell model. UOCV refers to the open-circuit voltage, R0 represents the series resistance, while R1 and C1 correspond to the dynamic resistance and dynamic capacitance, respectively [24], [25]. This model is widely used in battery management systems (BMS) and battery operation simulations [26], [27]. By knowing the parameters of the cell model, it is possible to estimate the state of charge (SOC) in real time [28], [29], [30]. Additionally, with knowledge of the energy consumption profile, it becomes feasible to optimally select a battery [31].

OCV (Open Circuit Voltage), is a fundamental parameter characterizing lithium-ion batteries. It is the

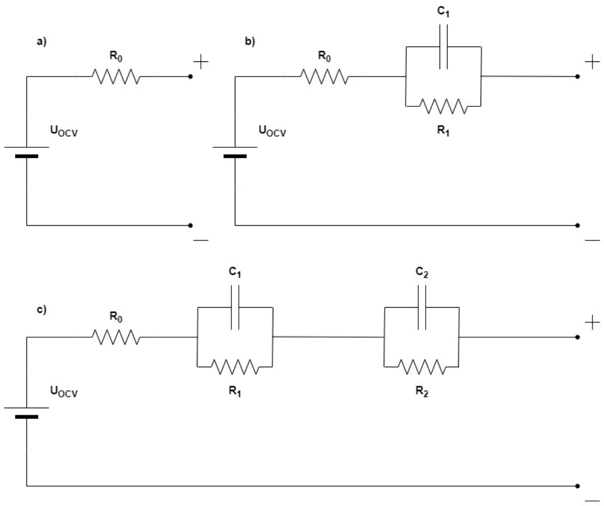

Fig. 3. Equivalent Cell Model: a) Series, b) First-order, c) Second-order.

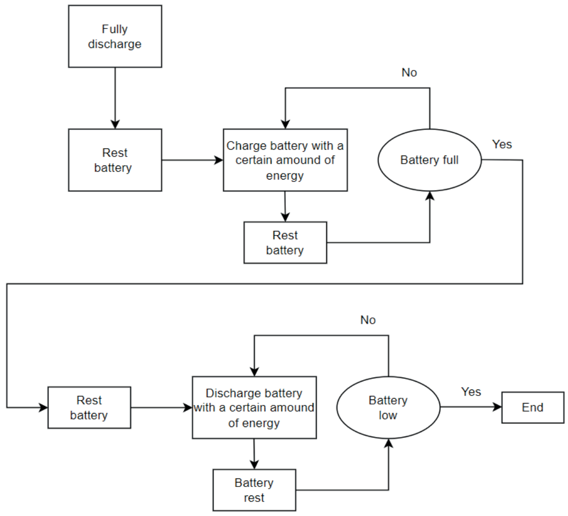

Fig. 4. Procedure for determining the OCV-SOC curve of a cel.

voltage measured at the cell's terminals when the battery is at rest, with no current flowing through it (neither discharge nor charge). The relationship between OCV and SOC is not linear — in typical lithium-ion batteries, it exhibits a gently curved profile, with more pronounced voltage differences at lower or higher SOC levels.

(1) $$V_{OCV}(s) = SOC(s)$$

where: s∈[0,1] and mean state of charge battery.[32]

One of the methods for determining the OCV-SOC characteristic is to experimentally establish the relationship by charging the cell with a small current of 1/20 C to the maximum cell voltage, then discharging it with the same current to the minimum voltage level, and subsequently determining the average values for the corresponding state of charge levels [33,34].

Another method is conducting the Hybrid Pulse Power Characterization (HPPC) test shown in the graph in Figure 4. This is a technique for examining cell properties, allowing for the assessment of their performance under various load conditions and at different stages of the lifecycle. The test involves applying a series of current pulses with varying intensities to the cell, during both charging and discharging phases. Throughout the test, voltage, current, and temperature of the cell are measured. The HPPC test is performed under controlled conditions, typically in research laboratories, and encompasses various battery state-of-charge (SOC) levels [35]. It is widely used for evaluating energy storage systems in electric vehicles, ensuring their compatibility with high-power demands and efficiency standards. To determine the OCV values for specific SOC levels, studies were conducted according to the following algorithm [36].

Internal resistance is a key parameter defining the power, energy efficiency, and heat losses of a lithium-ion cell. Accurate knowledge of this value is essential when designing battery systems for automotive applications [37,38]. Generally, the internal resistance of a battery increases as it degrades, which can negatively affect its performance due to energy losses caused by Joule heating and a drop in discharge voltage. Furthermore, since a battery's internal resistance can vary due to manufacturing issues, it is widely considered a critical evaluation factor in most battery production processes [39]. The primary method for determining a cell's series resistance involves applying a known current load and recording the resulting voltage change across the cell [40]. Based on these measurements, the resistance value can be calculated using the formula:

(2) $$R_0 = \frac{V_{OCV} - V_{OBC}}{\triangle I}$$

This method allows for quick results but requires a precise measurement of both current and voltage. Additionally, the measurement must be performed for each SOC level for which the resistance value is sought. Another method for determining series resistance is conducting the HPPC test [41,42], following the procedure outlined in the earlier part of this article.

(3) $$R_0 = \frac{\triangle V_1 - \triangle V_2}{2\triangle I}$$

Another approach is to perform a direct measurement of internal resistance using dedicated devices [43,44]. For this purpose, measurements should be taken at various SOC levels of the cell, ensuring that other devices are disconnected from the tested cell and do not affect the obtained result.

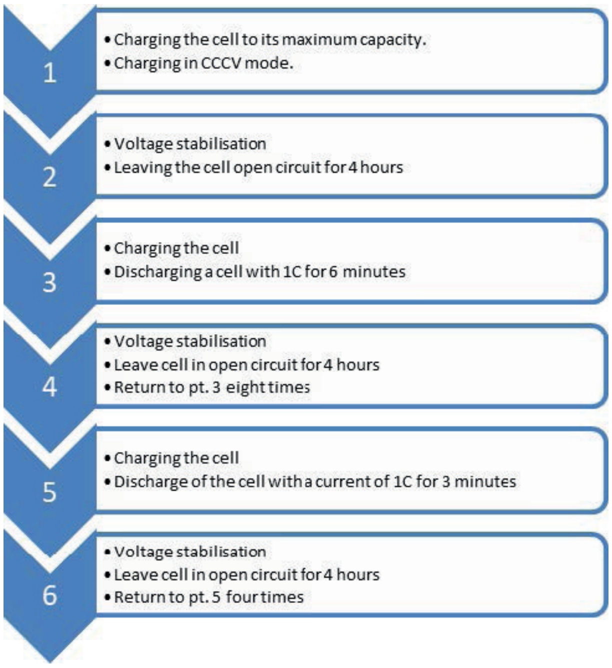

Fig. 5. Algorithm of the battery test.

Figure 6 shows a diagram of the measurement set-up for directly measuring the series resistance using the four-wire method [44].

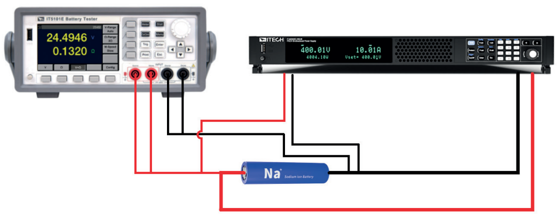

Fig. 6. Voltage and Resistance Measurement of a Sodium-Ion Cell Using the Four-Wire Method.

Table 1. Catalogue data of the IT-M3904C-80-80.

Parameter	Value
Maximum current (A)	±80
Maximum voltage (V)	±80
Internal resistance (Ω)	0,001
Resolution of voltage reading (%)	0,03
Resolution of current reading (%)	0,1

Table 2. Catalogue data of the IT5101.

Parameter	Value
Used voltage measurement range (V)	±6
Resolution of voltage reading (%)	0,4
Used resistance measurement range (mΩ)	±30
Resolution of resistance reading (μΩ)	1

Dynamic Branch - This is a parallel connection of resistor R1 and capacitor C1 [45,46], which models the dynamic behavior of the cell associated with the electrochemical processes occurring within the battery [47]. Dynamic resistance arises from polarization processes and internal resistances, accounting for energy losses caused by chemical reactions inside the battery. Dynamic capacitance relates to the charge storage effect associated with the double layer at the electrode-electrolyte interface. It models the delay in the voltage response to changes in load current. The literature also references the parameter τ, which is the product of R1 and C1. It indicates how quickly the voltage stabilizes after a dynamic change in load current. The larger this product, the slower the dynamic processes.

These values can be determined by analyzing the voltage response of the cell to changes in load current. An example of the voltage profile during an HPPC test is shown in Figure 7. Time t_0 refers to the start of the load change, while time t_1 corresponds to the voltage drop across the series resistance in the cell's equivalent model. Time t_2 is used to determine the first-order dynamic parameters. For this purpose, the voltage graph from the HPPC test [48,49], described earlier in this article, can be analyzed. The dynamic resistance for the first-order model can be calculated using the following formula [50]:

(4) $$R_1 = \frac{V_b(t_2) - \triangle V_b(t_1)}{\triangle I}$$

And the dynamic capacity from the formula:

(5) $$C_1 = \frac{\tau_1}{R_1}$$

Experiment

The experiments aimed at creating the equivalent cell model were conducted on a sodium-ion cell, SEEKWATT 18650CYA, with parameters shown in Table 3.

Table 3. Catalogue data of the cell under test.

Parameter	Value
Nominal energy Capacity (mAh)	1300
Nominal voltage (V)	3,1
Internal resistance (mΩ)	<20
Maximum cell voltage (V)	3,95
Minimum cell voltage (V)	1,5
Weight (g)	30
Maximum temperature (°C)	60
Minimum temperature(°C)	-30

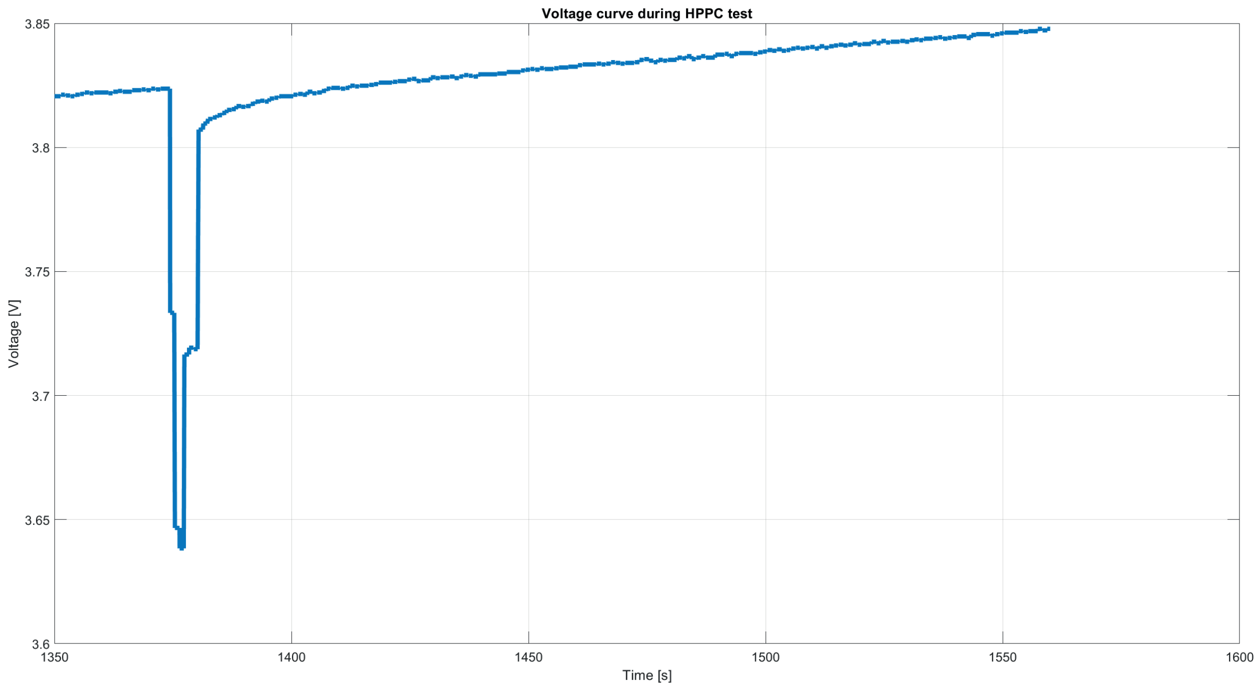

Fig. 7. Voltage and current curve during HPPC test. [48]

Test bench comprising the ITECH IT-M3904 programmable bi-directional power supply, the ITECH IT5101 cell tester and a PC for acquisition and processing of measurement data.

The measurements were conducted at room temperature, after which the cell was placed in a thermal chamber maintaining a constant ambient temperature of -15°C. Once the cell was cooled, the test was repeated, and the obtained profiles are shown in Figure 9.

Next, the tested cell was discharged to its minimum operating voltage using the CCCV method, reaching a voltage of 1.5V. An HPPC test was then conducted, after which the cell was discharged again and subsequently charged to specific SOC levels. Following a relaxation period, the voltage was measured. The determined curves are presented in Figure 10

The cell was then discharged again, after which it was charged to specific SOC levels. A direct meas-

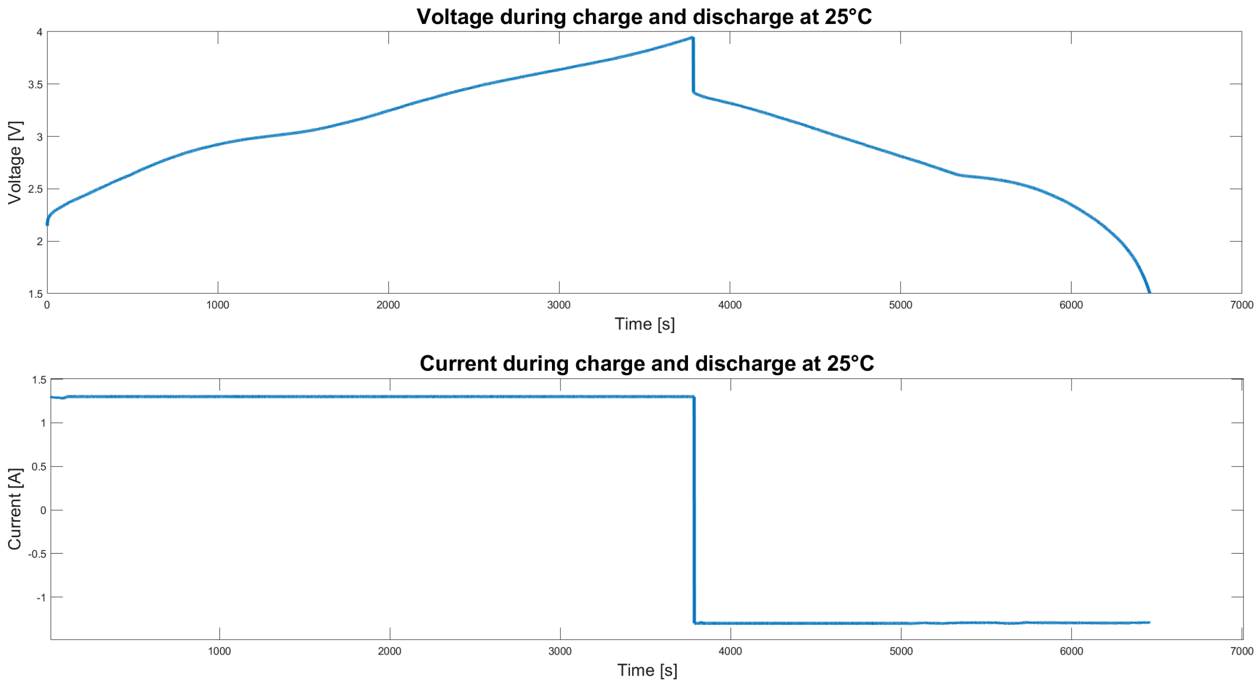

Fig. 8. Measured voltage and current during charge and discharge at 25°C.

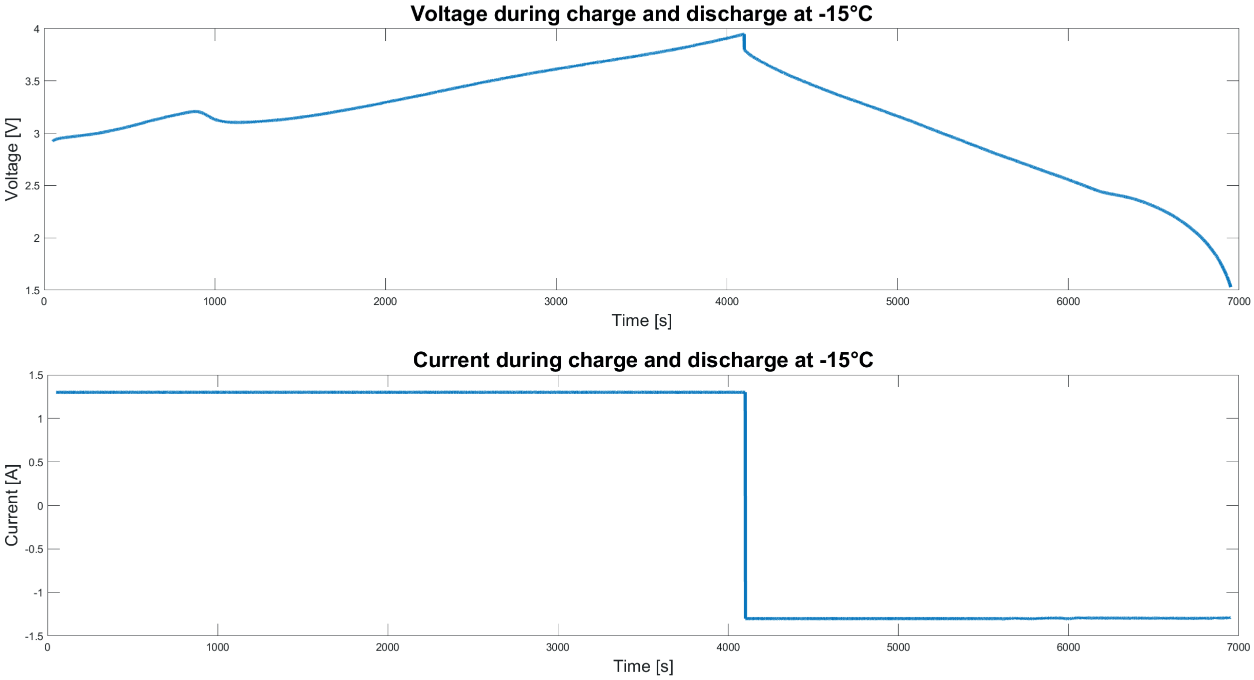

Fig. 9. Measured voltage and current during charge and discharge at -15℃.

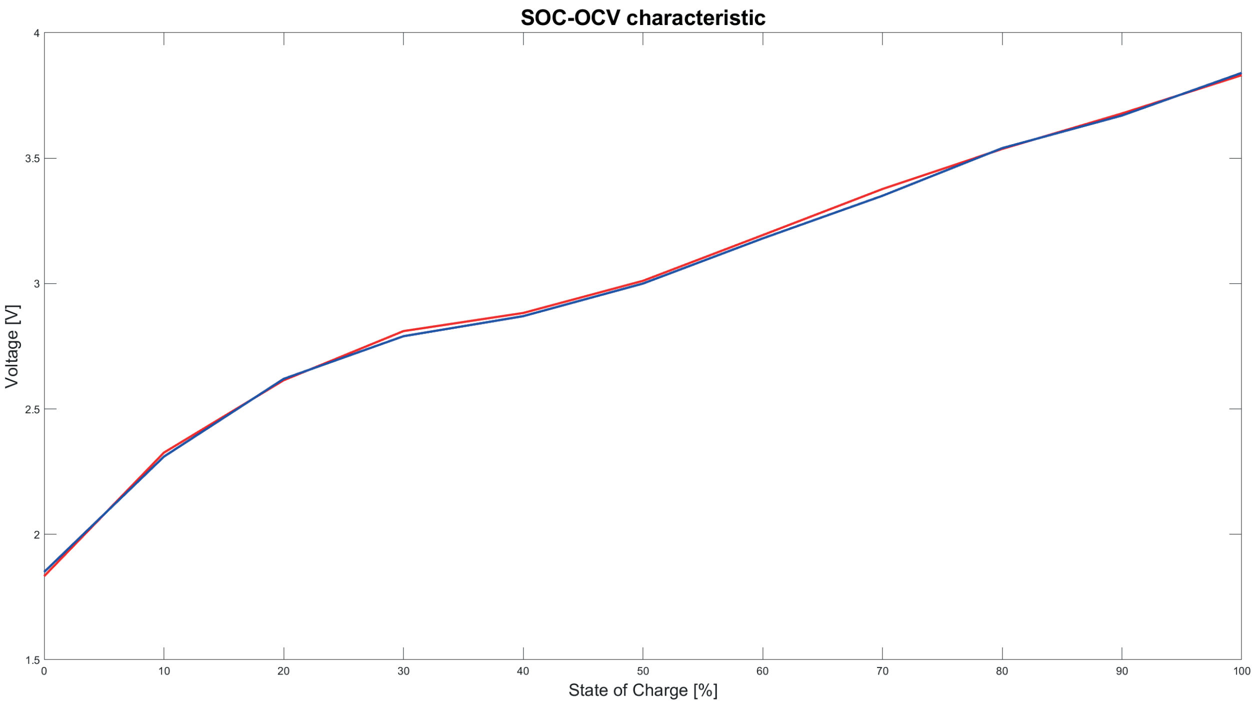

Fig. 10. OCV-SOC curve determined analytically from HPPC test results (red) and experimentally using voltage measurement (blue).

urement of the cell's internal resistance was then performed using the ITECH IT5101 battery tester. The results obtained for each SOC level were averaged and then compared with the results obtained analytically from the previously conducted HPPC test.

Figure 11 presents the results of the series resistance measurements of a sodium-ion cell. Data analysis indicates a low value of series resistance, which is a favorable indicator of high ionic conductivity of the electrolyte and effective electrical contact between the cell components. The stability of the series resistance values over the tested time range suggests good electrode stability. The obtained results confirm the optimality of the material and structural configuration of the cell, which contributes to minimizing resistive losses and improving the energy efficiency of the system.

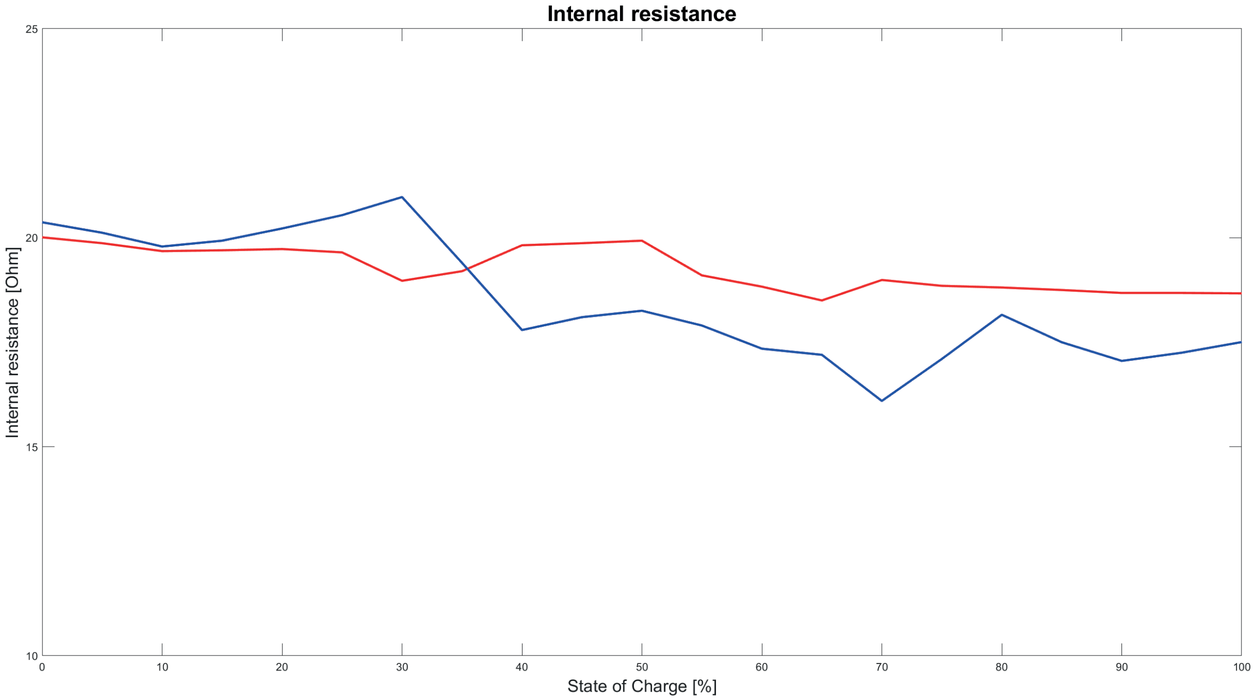

Fig. 11. The series resistance curve of the cell as a function of SOC, determined analytically based on the results of the HPPC test (red color) and experimentally using the ITECH IT5101 battery tester (blue color)

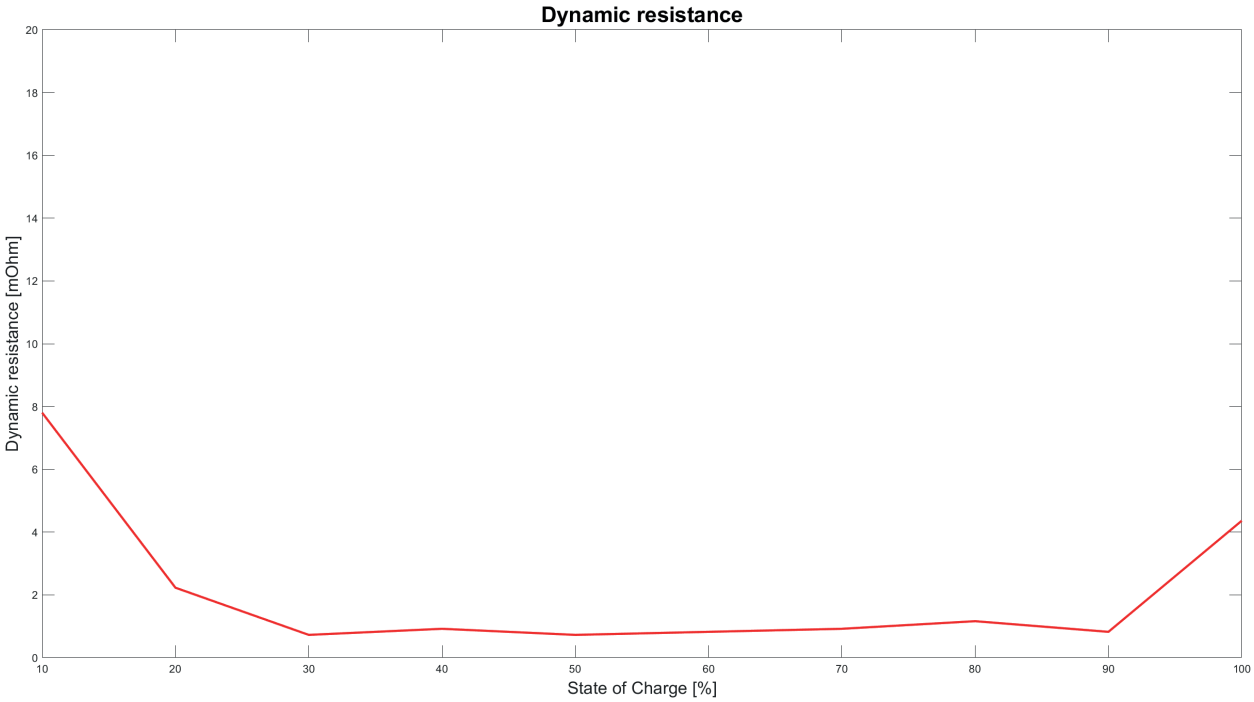

Fig. 12. The dynamic resistance curve of the cell as a function of SOC, determined analytically based on the results of the HPPC test

Figure 12 illustrates the variation of the dynamic resistance of the system as a function of the state of charge. In the initial charging stages, the dynamic resistance remains at a relatively high level, which may be related to limited conductivity at low voltage and transient phenomena in the active material structure. As the state of charge increases, a clear decrease in resistance is observed, indicating improved conduction conditions and system stabilization. This is significant from the perspective of energy efficiency, as lower dynamic resistance directly translates into reduced heat losses and higher energy conversion efficiency.

Figure 13, in turn, presents the characteristic of dynamic capacitance, which exhibits a nonlinear dependence on the voltage level. Capacitance values are significantly higher in the mid-voltage range, which may

PRZEGLĄD ELEKTROTECHNICZNY
OPEN ACCESS

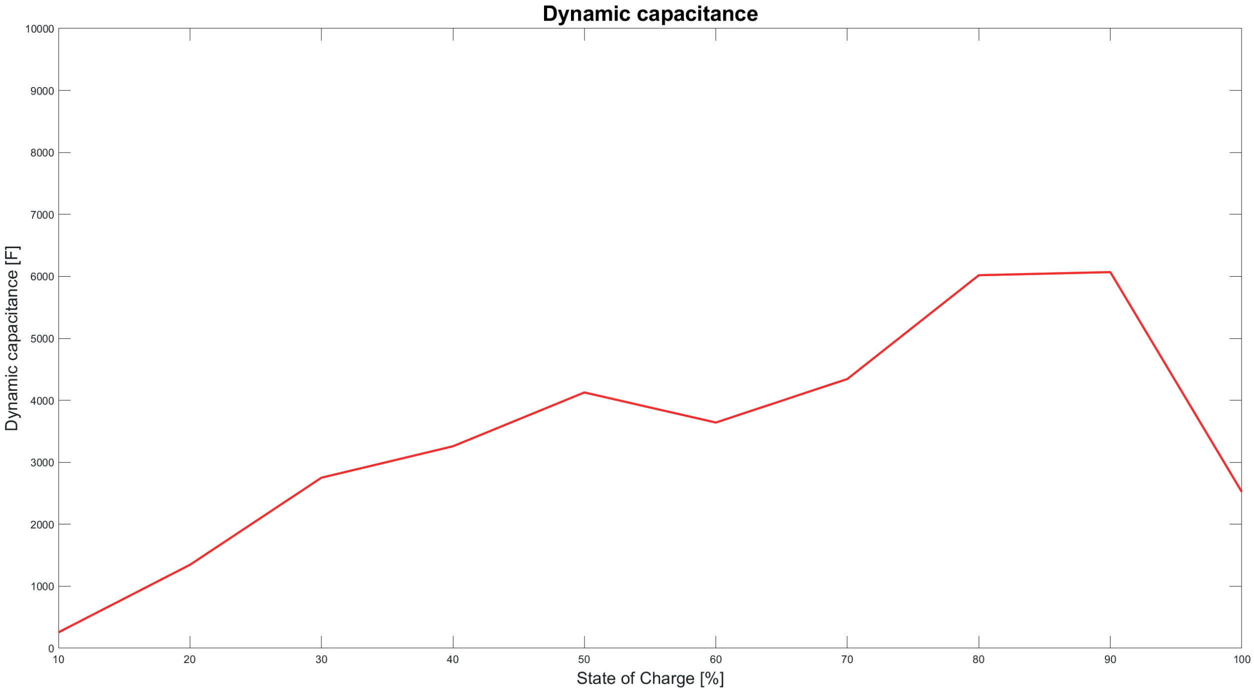

Fig. 13. The dynamic capacitance curve of the cell as a function of SOC, determined analytically based on the results of the HPPC test

indicate an increased charge storage capacity within this operating window. This effect may result both from the dielectric properties of the materials used and from geometric aspects of the system (e.g., variable electric field or the shape of conductive layers). The combined analysis of both parameters—dynamic resistance and capacitance—allows for a comprehensive understanding of the dynamic characteristics of the examined system. Their mutual dependencies highlight the complex nature of energy storage and conduction processes and enable assessment of the system's stability and efficiency under various operating conditions. Such analysis is particularly valuable in the context of energy optimization of converters, where precise tuning of dynamic parameters can significantly impact their final performance and operational reliability in practical applications.

The values of the dynamic parameters can only be determined using analytical methods. For this purpose, the previously obtained HPPC test results were analyzed, and based on them, the values of dynamic resistance and dynamic capacitance were calculated. The voltage graph during the test is shown in Figure 14.

Conclusions

In this study, a battery model for a sodium-ion cell with a capacity of 1300 mAh was developed. To determine the model parameters, a series of experiments were conducted on the cell. These parameters can also be determined using other methods, which will be explored in future studies; however, this is beyond the scope of the current work. To parameterize the sodium-ion battery model, it was necessary to define the key performance parameters of this type of cell. The model proved capable of accurately reproducing the cell voltage across a wide range of operating conditions. Internal resistance, open circuit voltage, and cell capacity were measured at various state-of-charge (SOC) levels, temperatures, and load currents. The developed model should allow for precise prediction of the cell voltage behavior under both high and low load currents. Experimental results were compared with simulation results, which allowed for the assessment of the accuracy of the parameterized and proposed model for the studied sodium-ion cell. The model's accuracy was evaluated through a series of validation experiments. The developed sodium-ion cell model can be implemented into a Battery Management System (BMS) module, ensuring safety in electromobility systems as well as in stationary energy storage systems.

Received: 05.02.2025, **Accepted:** 05.08.2025, **Published:** 29.08.2025

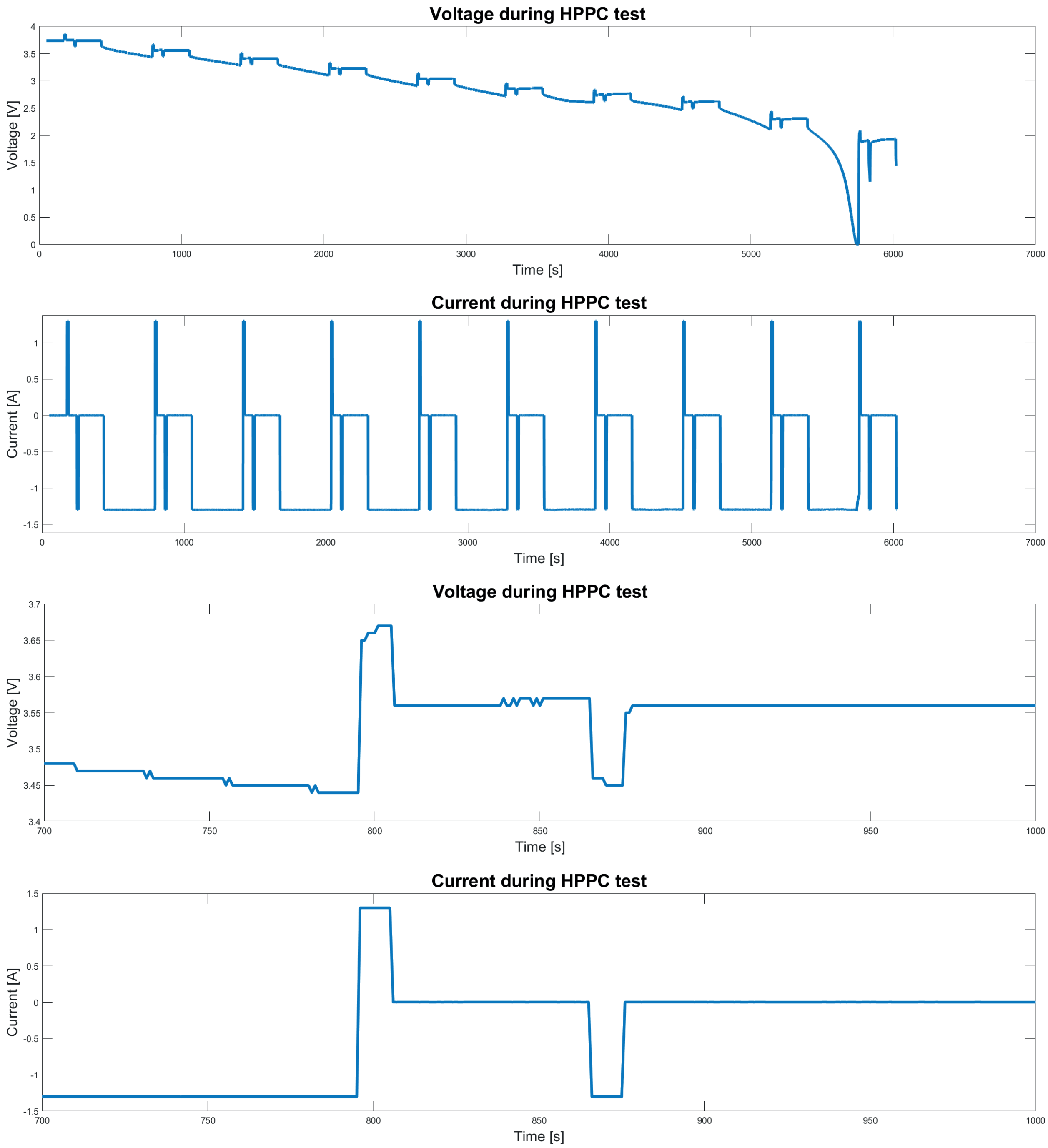

Fig. 14. Voltage curve recorded during the HPPC test.

REFERENCES

[1] Piasecki S, Bachman S, Zaleski J, Jasinski M, Turzyński M. AC-DC-DC Converter for Small Power Energy Storage Systems. Energies. 2023; 16(22):7556. https://doi.org/10.3390/en16227556

[2] Martínez-Caballero, L.; Kot, R.; Milczarek, A.; Malinowski, M. Comparison of Energy Storage Management Techniques for a Grid-Connected PV- and Battery-Supplied Residential System. Electronics 2024, 13, 87. https://doi.org/10.3390/electronics13010087

[3] M. Gharebaghi, O. Rezaei, C. Li, Z. Wang, i Y. Tang, „A Survey on Using Second-Life Batteries in Stationary Energy Storage Applications”, Energies, t. 18, nr 1, Art. nr 1, sty. 2025, doi: 10.3390/en18010042.

[4] Y.-S. Hu i Y. Li, „Unlocking Sustainable Na-Ion Batteries into Industry”, ACS Energy Lett., t. 6, nr 11, s. 4115–4117, lis. 2021, doi: 10.1021/acsenergylett.1c02292.

[5] H. Fatima, Y. Zhong, H. Wu, i Z. Shao, „Recent advances in functional oxides for high energy density sodium-ion

batteries”, Materials Reports: Energy, t. 1, nr 2, s. 100022, maj 2021, doi: 10.1016/j.matre.2021.100022.
[6] A. Rudola i in., „Commercialization of high energy density sodium-ion batteries: Faradion’s journey and outlook”, J. Mater. Chem. A, t. 9, nr 13, s. 8279–8302, kwi. 2021, doi: 10.1039/D1TA00376C.
[7] W. Luo, S. Stynski, A. Chub, L. G. Franquelo, M. Malinowski and D. Vinnikov, “Utility-Scale Energy Storage Systems: A Comprehensive Review of Their Applications, Challenges, and Future Directions,” in IEEE Industrial Electronics Magazine, vol. 15, no. 4, pp. 17-27, Dec. 2021, doi: 10.1109/MIE.2020.3026169.
[8] Li-Ion Cell Operation at Low Temperatures - IOPscience”. Dostęp: 1 styczeń 2025. [Online]. Dostępne na: https://iopscience.iop.org/article/10.1149/2.047304jes/meta
[9] G. Zhang, S. Ge, T. Xu, X.-G. Yang, H. Tian, i C.-Y. Wang, „Rapid self-heating and internal temperature sensing of lithium-ion batteries at low temperatures”, Electrochimica Acta, t. 218, s. 149–155, lis. 2016, doi: 10.1016/j.electacta.2016.09.117.
[10] Z. Li i in., „Sodium-Ion Battery with a Wide Operation-Temperature Range from −70 to 100 °C”, Angewandte Chemie International Edition, t. 61, nr 13, Art. nr 13, 2022, doi: 10.1002/anie.202116930.
[11] K. Zhu, Z. Sun, Z. Li, P. Liu, X. Chen, i L. Jiao, „Aqueous sodium ion hybrid batteries with ultra-long cycle life at -50 °C”, Energy Storage Materials, t. 53, s. 523–531, grudz. 2022, doi: 10.1016/j.ensm.2022.09.019.
[12] Z. Li i in., „Thermal runaway comparison and assessment between sodium-ion and lithium-ion batteries”, Process Safety and Environmental Protection, t. 193, s. 842–855, sty. 2025, doi: 10.1016/j.psep.2024.11.118.
[13] J. B. Robinson i in., „Multiscale tomographic analysis of the thermal failure of Na-Ion batteries”, Journal of Power Sources, t. 400, s. 360–368, paź. 2018, doi: 10.1016/j.jpowsour.2018.07.098.
[14] Z. Tang, A. Song, S. Wang, J. Cheng, i C. Tao, „Numerical Analysis of Heat Transfer Mechanism of Thermal Runaway Propagation for Cylindrical Lithium-ion Cells in Battery Module”, Energies, t. 13, nr 4, Art. nr 4, sty. 2020, doi: 10.3390/en13041010.
[15] S. Mallick i D. Gayen, „Thermal behaviour and thermal runaway propagation in lithium-ion battery systems – A critical review”, Journal of Energy Storage, t. 62, s. 106894, cze. 2023, doi: 10.1016/j.est.2023.106894.
[16] Y. Fedoryshyna, S. Schaeffler, J. Soellner, E. I. Gillich, i A. Jossen, „Quantification of venting behavior of cylindrical lithium-ion and sodium-ion batteries during thermal runaway”, Journal of Power Sources, t. 615, s. 235064, wrz. 2024, doi: 10.1016/j.jpowsour.2024.235064.
[17] K. Sirengo, A. Babu, B. Brennan, i S. C. Pillai, „Ionic liquid electrolytes for sodium-ion batteries to control thermal runaway”, Journal of Energy Chemistry, t. 81, s. 321–338, cze. 2023, doi: 10.1016/j.jechem.2023.02.046.
[18] Y. Sun, P. Shi, H. Xiang, X. Liang, i Y. Yu, „High-Safety Nonaqueous Electrolytes and Interphases for Sodium-Ion Batteries”, Small, t. 15, nr 14, s. 1805479, 2019, doi: 10.1002/smll.201805479.
[19] C. Yang, S. Xin, L. Mai, i Y. You, „Materials Design for High-Safety Sodium-Ion Battery”, Advanced Energy Materials, t. 11, nr 2, s. 2000974, 2021, doi: 10.1002/aenm.202000974.
[20] T. Białoń, R. Niestrój, i W. Korski, „PSO-Based Identification of the Li-Ion Battery Cell Parameters”, Energies, t. 16, nr 10, Art. nr 10, sty. 2023, doi: 10.3390/en16103995.
[21] G. Saldaña, J. I. San Martín, I. Zamora, F. J. Asensio, i O. Oñederra, „Analysis of the Current Electric Battery Models for Electric Vehicle Simulation”, Energies, t. 12, nr 14, Art. nr 14, sty. 2019, doi: 10.3390/en12142750.
[22] S. Tamilselvi i in., „A Review on Battery Modelling Techniques”, Sustainability, t. 13, nr 18, Art. nr 18, sty. 2021, doi: 10.3390/su131810042.
[23] A. S. Pande, B. P. Soni, i K. V. Bhadane, „Electrical Models for EV’s Batteries: An Overview and Mathematical Design of RC Network”, J. Inst. Eng. India Ser. B, t. 104, nr 2, s. 533–547, kwi. 2023, doi: 10.1007/s40031-022-00852-1.
[24] A. S. Pande, B. P. Soni, K. V. Bhadane, i A. Mukherjee, „BATTERIES: CLASSIFICATION AND REVIEW OF ELECTRIC CIRCUIT MODELS FOR ELECTRIC VEHICLE”.
[25] H. Zhang i in., „Effect of Sample Interval on the Parameter Identification Results of RC Equivalent Circuit Models of Li-ion Battery: An Investigation Based on HPPC Test Data”, Batteries, t. 9, nr 1, Art. nr 1, sty. 2023, doi: 10.3390/batteries9010001.
[26] P. Makeen, H. A. Ghali, i S. Memon, „A Review of Various Fast Charging Power and Thermal Protocols for Electric Vehicles Represented by Lithium-Ion Battery Systems”, Future Transportation, t. 2, nr 1, Art. nr 1, mar. 2022, doi: 10.3390/futuretransp2010015.
[27] A. Baczyńska, W. Niewiadomski, A. Gonçalves, P. Almeida, i R. Luís, „Li-NMC Batteries Model Evaluation with Experimental Data for Electric Vehicle Application”, Batteries, t. 4, nr 1, Art. nr 1, mar. 2018, doi: 10.3390/batteries4010011.
[28] „Comparative Research on RC Equivalent Circuit Models for Lithium-Ion Batteries of Electric Vehicles”. Dostęp: 19 grudzień 2024. [Online]. Dostępne na: https://www.mdpi.com/2076-3417/7/10/1002
[29] Z. He, D. Martín Gómez, A. de la Escalera Hueso, P. Flores Peña, X. Lu, i J. M. Armingol Moreno, „Battery-SOC Estimation for Hybrid-Power UAVs Using Fast-OCV Curve with Unscented Kalman Filters”, Sensors, t. 23, nr 14, Art. nr 14, sty. 2023, doi: 10.3390/s23146429.
[30] D. Ge, Z. Zhang, X. Kong, i Z. Wan, „Online SoC Estimation of Lithium-Ion Batteries Using a New Sigma Points Kalman Filter”, Applied Sciences, t. 11, nr 24, Art. nr 24, sty. 2021, doi: 10.3390/app112411797.
[31] Q. Lin, X. Li, B. Tu, J. Cao, M. Zhang, i J. Xiang, „Stable and Accurate Estimation of SOC Using eXogenous Kalman Filter for Lithium-Ion Batteries”, Sensors, t. 23, nr 1, Art. nr 1, sty. 2023, doi: 10.3390/s23010467.
[32] C. Imane, „ANN approach to SOC estimation of Lithium-Ion Battery”, Przegląd Elektrotechniczny, t. 1, nr 8, s. 200–202, sie. 2024, doi: 10.15199/48.2024.08.41.
[33] B. Pattipati, B. Balasingam, G. V. Avvari, K. R. Pattipati, i Y. Bar-Shalom, „Open circuit voltage characterization of lithium-ion batteries”, Journal of Power Sources, t. 269, s. 317–333, grudz. 2014, doi: 10.1016/j.jpowsour.2014.06.152.
[34] C. Zhang, J. Jiang, L. Zhang, S. Liu, L. Wang, i P. C. Loh, „A Generalized SOC-OCV Model for Lithium-Ion Batteries and the SOC Estimation for LNMCO Battery”, Energies, t. 9, nr 11, Art. nr 11, lis. 2016, doi: 10.3390/en9110900.
[35] P. Pillai, S. Sundaresan, P. Kumar, K. R. Pattipati, i B. Balasingam, „Open-Circuit Voltage Models for Battery Management Systems: A Review”, Energies, t. 15, nr 18, Art. nr 18, sty. 2022, doi: 10.3390/en15186803.

[36] T. Białoń, R. Niestrój, W. Skarka, i W. Korski, „HPPC Test Methodology Using LFP Battery Cell Identification Tests as an Example", Energies, t. 16, nr 17, Art. nr 17, sty. 2023, doi: 10.3390/en16176239.

[37] P. Gałuszkiewicz, „Magazynowanie energii w magazynach elektrochemicznych w oparciu o akumulatory LiFePO4 i LTO", ELECTROTECHNICAL REVIEW, t. 1, nr 4, s. 203–206, kwi. 2024, doi: 10.15199/48.2024.04.38.

[38] H.-G. Schweiger i in., „Comparison of Several Methods for Determining the Internal Resistance of Lithium Ion Cells", Sensors, t. 10, nr 6, Art. nr 6, cze. 2010, doi: 10.3390/s100605604.

[39] B. V. Ratnakumar, M. C. Smart, L. D. Whitcanack, i R. C. Ewell, „The impedance characteristics of Mars Exploration Rover Li-ion batteries", Journal of Power Sources, t. 159, nr 2, s. 1428–1439, wrz. 2006, doi: 10.1016/j.jpowsour.2005.11.085.

[40] M.-G. Lim, J.-B. Jung, N.-H. Kim, J.-M. Kim, J. Shen, i D.-S. Rho, „Evaluation Method of Internal Resistance for Repurposing Using Middle and Large-Sized Batteries", Energies, t. 16, nr 15, Art. nr 15, sty. 2023, doi: 10.3390/en16155652.

[41] M. Mathew, S. Janhunen, M. Rashid, F. Long, i M. Fowler, „Comparative Analysis of Lithium-Ion Battery Resistance Estimation Techniques for Battery Management Systems", Energies, t. 11, nr 6, Art. nr 6, cze. 2018, doi: 10.3390/en11061490.

[42] M.-K. Tran, A. DaCosta, A. Mevawalla, S. Panchal, i M. Fowler, „Comparative Study of Equivalent Circuit Models Performance in Four Common Lithium-Ion Batteries: LFP, NMC, LMO, NCA", Batteries, t. 7, nr 3, Art. nr 3, wrz. 2021, doi: 10.3390/batteries7030051.

[43] H. He, R. Xiong, i J. Fan, „Evaluation of Lithium-Ion Battery Equivalent Circuit Models for State of Charge Estimation by an Experimental Approach", Energies, t. 4, nr 4, Art. nr 4, kwi. 2011, doi: 10.3390/en4040582.

[44] N. Islam, „Calibration and Testing Methodology of Mobile Battery Systems".

[45] Y. Liu, J.-R. Riba, i M. Moreno-Eguilaz, „Energy Balance of Wireless Sensor Nodes Based on Bluetooth Low Energy and Thermoelectric Energy Harvesting", Sensors, t. 23, nr 3, Art. nr 3, sty. 2023, doi: 10.3390/s23031480.

[46] D. Salazar i M. Garcia, „Estimation and Comparison of SOC in Batteries Used in Electromobility Using the Thevenin Model and Coulomb Ampere Counting", Energies, t. 15, nr 19, Art. nr 19, sty. 2022, doi: 10.3390/en15197204.

[47] G. Barletta, P. DiPrima, i D. Papurello, „Thévenin's Battery Model Parameter Estimation Based on Simulink", Energies, t. 15, nr 17, Art. nr 17, sty. 2022, doi: 10.3390/en15176207.

[48] G. Saldaña, J. I. San Martín, I. Zamora, F. J. Asensio, i O. Oñederra, „Analysis of the Current Electric Battery Models for Electric Vehicle Simulation", Energies, t. 12, nr 14, Art. nr 14, sty. 2019, doi: 10.3390/en12142750.

[49] A. Suti, G. Di Rito, i G. Mattei, „Development and Experimental Validation of Novel Thevenin-Based Hysteretic Models for Li-Po Battery Packs Employed in Fixed-Wing UAVs", Energies, t. 15, nr 23, Art. nr 23, sty. 2022, doi: 10.3390/en15239249.

[50] D. Gandolfo, A. Brandão, D. Patiño, i M. Molina, „Dynamic model of lithium polymer battery – Load resistor method for electric parameters identification", Journal of the Energy Institute, t. 88, nr 4, s. 470–479, lis. 2015, doi: 10.1016/j.joei.2014.10.004.

[51] S. S. Madani, E. Schaltz, i S. Knudsen Kær, „An Electrical Equivalent Circuit Model of a Lithium Titanate Oxide Battery", Batteries, t. 5, nr 1, Art. nr 1, mar. 2019, doi: 10.3390/batteries5010031.